In silico drug repositioning against human NRP1 to block SARS-CoV-2 host entry

Şeref GÜL

Department of Chemical and Biological Engineering, KOÇ University, İstanbul, Turkey

*Correspondence: serefgul@ku.edu.tr

Abstract

Despite COVID-19 turned into a pandemic, no approved drug for the treatment or globally available vaccine is out yet. In such a global emergency, drug repurposing approach that bypasses a costly and long-time demanding drug discovery process is an effective way in search of finding drugs for the COVID-19 treatment. Recent studies showed that SARS-CoV-2 uses neuropilin-1 (NRP1) for host entry. Here I took advantage of structural information of the NRP1 in complex with C-terminal of spike (S) protein of SARS-CoV-2 to identify drugs that may inhibit NRP1 and S protein interaction. U.S. Food and Drug Administration (FDA) approved drugs were screened using docking simulations. Among top drugs, well-tolerated drugs were selected for further analysis. Molecular dynamics (MD) simulations of drugs-NRP1 complexes were run for 100 ns to assess the persistency of binding. MM/GBSA calculations from MD simulations showed that eltrombopag, glimepiride, sitagliptin, dutasteride, and ergotamine stably and strongly bind to NRP1. In silico Alanine scanning analysis revealed that Tyr^{297}, Trp^{301}, and Tyr^{353} amino acids of NRP1 are critical for drug binding. Validating the effect of drugs analyzed in this paper by experimental studies and clinical trials will expedite the drug discovery process for COVID-19.

1.   Introduction

Severe acute respiratory syndrome coronavirus 2 (SARS-CoV-2) infected over 40 million people and resulted in more than 1.5 million deaths around the world since December 2019[*]. The coronavirus disease-2019 (COVID-19) has symptoms of pneumonia manifesting fever, fatigue, dyspnea, chest pain, and cough which are also observed in other viral respiratory diseases (Yi et al., 2020). The whole-genome analysis showed that SARS-CoV-2 belongs to the *Betacoronovirus* genera and has a 96% genomic sequence identity to that of bat coronavirus (Wu et al., 2020b; Zhou et al., 2020). Despite the high genomic similarities, SARS-CoV-2 behaves more aggressively than SARS-CoV in terms of viral load, reaching the peak RNA concentration, tissue tropism, and transmission efficiency (Wolfel et al., 2020).

SARS-CoV-2 genome is composed of a (+) sense single-strand RNA (ssRNA) with 14 open reading frames (ORFs). SARS-CoV-2 synthesizes two polyproteins, ORF1a and ORF1ab, and four structural proteins e.g. spike (S), envelop (E), matrix (M), and nucleocapsid (N) proteins and accessory proteins (3a, 3b, p6, 7a, 7b, 8b, 9b, and orf14) (Wu et al., 2020a; Yoshimoto, 2020). Proteolytic cleavage of ORF1a and ORF1ab by proteases leads to the production of 16 non-structural proteins (nsps). Among nsps, nsp5 (3C-like protease, 3CL^{pro}) first cleaves its bounds with nsp4 and nsp6, then cleaves the ORF1a and ORF1ab at 11 sites (Du et al., 2004; Muramatsu et al., 2013). Besides 3CL^{pro}, nsp3 (papain-like protease, PL^{pro}) cleaves these polyproteins at three sites and completes the production of 16 nsps (Baez-Santos et al., 2015; Thiel et al., 2003).

---

[*] Worldometers (2020) Website: https://www.worldometers.info/coronavirus/ [accessed 05 December 2020]

S protein of SARS-CoV-2 interacts with angiotensin-converting enzyme 2 (ACE2) that has been accepted as the main receptor for the entry of the virus (Wang et al., 2020; Yan et al., 2020). ACE2, a membrane protein, is expressed in lung, upper and stratified epithelial cells of the esophagus, heart, kidney, testis, colon, ileum, and intestine (Donoghue et al., 2000; Zhang et al., 2020). Despite the attenuated expression of ACE2 in elderly people, increased or unaffected severity of COVID-19 symptoms (Walls et al., 2020) in these people (Liu et al., 2020; Omori et al., 2020; Singh et al., 2020a), and high viral loads in the throat (Wolfel et al., 2020) suggest the existence of an alternative receptor for the virus entry.

A polybasic sequence (Arg^{682}Arg-Ala-Arg^{685}) at the S1/S2 region of S protein of the SARS-CoV-2 may explain its higher transmission rate and tissue tropism. This sequence is also conserved in the S protein of various pathogenic human viruses such as Ebola, influenza, and HIV-1 (Tse et al., 2014). Cleavage of the S protein within the polybasic sequence, which is primed by transmembrane serine protease 2 (TMPRSS2) via furin produces S1 and S2 (Hoffmann et al., 2020b). *FURIN* mediated cleavage of S protein results in increased tropism and the infection rate of SARS-CoV-2, most probably because of the formation of new cell surface binding regions (Hoffmann et al., 2020a; Wrapp et al., 2020). Knocking down *FURIN* gene or using its inhibitor decreases the virus entry to cells and syncytia formation in the infected cells, respectively (Shang et al., 2020; Walls et al., 2020).

(Arg^{682}Arg-Ala-Arg^{685}) sequence is aligned with [R/K]XX[R/K] motif (R:arginine, K:lysine, and X is any amino acid), named as 'C-end Rule' (CendR). CendR binds and activates cell surface receptors neuropilin (NRP1,2) (Teesalu et al., 2009). NRP1 binds to several growth factors such as vascular endothelial growth factors (VEGFs) (Soker et

al., 1998), hepatocyte growth factor (Sulpice et al., 2008), and transforming growth factor (Cao et al., 2010). Among those, the interaction between NRP1 and VEGF-A$_{165}$ has been extensively studied (Fantin et al., 2014; Jarvis et al., 2010; Jia et al., 2014; Mota et al., 2018; Parker et al., 2012; Powell et al., 2018; Teesalu et al., 2009). C-terminal arginine residue and CendR motif of VEGF-A$_{165}$ critically interact with b1 domain of NRP1 (NRP1-b1) in which natural and artificial NRP1 inhibitors were explored (Vander Kooi et al., 2007).

Recent studies showed that interaction between NRP1 and protein S of SARS-CoV-2 is required for the SARS-CoV-2 cell entry (Cantuti-Castelvetri et al., 2020; Daly et al., 2020). While co-expression of NRP1 with ACE2 and TMRPSS2 increased the infection, monoclonal antibody targeting the b1b2 extracellular domain of NRP1 significantly inhibited the infection. The stimulating effect of NRP1 on the virus infection diminished when the furin cleavage site of SARS-CoV-2 is mutated (Cantuti-Castelvetri et al., 2020). Analysis of direct interaction between CendR peptide of protein S and NRP1 using isothermal titration calorimetry method showed that binding affinity of the complex is between 20-13μM depending on the pH. Mutating the critical arginine residue (Arg^{685}) on the CendR of protein S attenuated the NRP1 binding (Daly et al., 2020). The crystallographic analysis confirmed that the binding mode of protein S' CendR to the NRP1 is similar to the previously resolved NRP1-VEGF-A structure (Daly et al., 2020; Parker et al., 2012).

To date, there is no consensus on the treatment of COVID-19 yet. Since developing a new drug is costly and requiring a long period, repurposing of U.S. Food and Drug Administration (FDA) approved drugs may provide an alternative approach to find a therapeutic for the COVID-19 treatment within a reasonable time and cost. Multiple

targets are available to neutralize COVID-19. For example, virus entry proteins on the host (ACE2, TMPRSS2, NRP1), replication machinery of the virus (3CL^{pro} RNA-dependent RNA polymerase), virus proteins taking roles on the assembly mechanism (protein E) and the release of the virus (protein M and N) are candidates for drug development and drug repurposing (Li et al., 2020a; Sarma et al., 2020; Schoeman and Fielding, 2019; Venkatagopalan et al., 2015). Given the crucial role of NRP1 for the SARS-CoV-2 entry into the host specifically in elderly people, this in silico study aimed to repurpose FDA-approved drugs against b1 domain of NRP1 to find a promising drug to block SARS-CoV-2 infection. For this purpose, I initially run docking simulations to find drugs with high binding affinity to b1 domain of NRP1. As a control, previously identified NRP1 inhibitor, EG01377, was docked to the same pocket. While docking binding energy of the inhibitor is around -6.0 kcal/mol, over 250 drugs have -7.4kcal/mol or lower Vina binding energy. Drugs were sorted based on docking binding energies, and an extensive literature search was done to select well-tolerated drugs for further analysis. 100 ns molecular dynamics simulations (MD) of drug-NRP1 complexes showed that thrombopoietin receptor agonist eltrombopag, migraine drug ergotamine, drugs for type 2 diabetes sitagliptin and glimepiride, and antiandrogen dutasteride can stably interact with NRP1. NRP1 in complex with EG01377 was simulated to compare the affinity of selected drugs with its inhibitor. Binding free energy calculation using MM/GBSA method showed that selected drugs have a comparable or better affinity to NRP1 than EG01377. Alanine scanning calculations revealed Tyr^{297}, Trp^{301}, and Tyr^{353} as the critical amino acid residues for drug-NRP1 interaction. These findings may be used in experimental studies and clinical trials to test the effect of promising drugs alone or in combination with current COVID-19 treatment protocols.

2.   Materials and methods

High-resolution human NRP1 structure (PDB ID: 6FMC) was retrieved from The Protein Data Bank (www.rcsb.org) (Powell et al., 2018). Protein was prepared for docking simulations via Dock Prep module of UCSF Chimera as described previously (Doruk et al., 2020; Gul et al., 2020; Tardu et al., 2016). Water molecules were removed and if alternate locations are available for residues, the ones with the higher occupancies were selected. Dunbrack 2010 rotamer library was used to complete missing side chains of amino acids, polar hydrogens were added, and non-polar hydrogens were merged with bound atoms. Atom charges should be defined to run docking simulations. Thus, Gasteiger charges to each atom in the protein were assigned using Auto Dock Tools (ADT) (v 1.5.6). Structures of drugs were downloaded from Zinc15 database catalogue of FDA-approved drugs. Set of drugs used in this study were imported from the U.S. Environmental Protection Agency's (EPA) Distributed Structure-Searchable Toxicity (DSSTox) database. The 3948 drugs and NRP1 inhibitor (EG01377) were prepared for docking by using ADT suite. Inhibitor binding pocket of NRP1 was targeted for docking simulations in which grid center was placed on the center of Tyr^{297}, Glu^{348}, and Tyr^{353} side chains with 6400 $Å^3$ of the grid box. AutoDock Vina (version 1.1.2) was used for the docking (http://vina.scripps.edu/) (Trott and Olson, 2010).

With the aid of VMD, NRP1 structure (PDB ID: 6FMC) was solvated using TIP3P water molecules in a rectangular box with a size of 4.50×10^5 $Å^3$. Solvated protein was neutralized and then ionized with sodium-chloride salt (Na^+ and Cl^-) to 150 mM final concentration to mimic the physiological conditions (Humphrey et al., 1996). 20000 steps of energy minimization (via conjugate gradient) was performed. The minimized system was gradually heated and then equilibrated for 1.4 ns (NPT ensemble) with constraints

on the protein. Constrains starting from 2 kcal/mol/Å^2 were reduced by 0.5 kcal/mol/Å^2 for each 0.4 ns equilibration run. Production simulation of 100 ns for each equilibrated drug-NRP1 complex was run using 2 fs time step at 310°K and 1atm pressure. Langevin thermostat and Langevin barostat maintained the temperature and pressure, respectively. To calculate the force acting on the system van der Waals (12Å cut-off) and long-range electrostatic interactions (via particle-mesh Ewald) were calculated. NAMD (Phillips et al., 2005) software and CHARMM36m forcefield (Huang et al., 2017) were used for all MD simulations. CHARMM-GUI server was used to generate parameters of drugs (Jo et al., 2008; Kim et al., 2017).

Analyses of protein-drug interactions were done by following these steps: 1) MD trajectory of each drug-protein simulation was visualized to inspect the position of the drug. If the drug leaves the binding pocket, that one is eliminated. 2) For simulations that drug-protein interaction was maintained for 100 ns, Root Mean Square Deviation (RMSD) of C$_\alpha$ atoms was calculated to verify the successful equilibration of the system. 3) Contact frequency between drug and nearby amino acid residues were carried out for determining the binding residues. 4) Binding free energy (BFE) of drugs was calculated using molecular mechanics generalized born surface area (MM/GBSA) method. 5) Amino acid residue with a high contact frequency was mutated to Alanine to calculate their contribution to BFE of drugs. All MD analyses were performed and protein figures were prepared by using VMD and Pymol, respectively (DeLano, 2009; Humphrey et al., 1996). RMSD trajectory tool and timeline function in VMD were used to calculate RMSD of protein and contact frequencies between drug and protein, respectively. Unstructured and highly dynamic first 9 N-terminal amino acid residues were excluded from the RMSD calculation.

For MM/GBSA and Alanine scanning calculations, MMPBSA.py script of AmberTools20 was used (Case et al., 2020). For each calculation, 25000 frames from 100 ns simulations were used. BFE between drug and protein is calculated based on Equation 1:

$$\Delta G_{binding} = G_{complex} - G_{receptor} - G_{ligand} \quad (1)$$

$G_{complex}$: Energy of protein-drug complex,

$G_{receptor}$: Energy of protein only

G_{ligand} : Energy of unbound drug

3.   Results

A To discover an antiviral drug diverse targets are available from viral replication enzymes to host proteins facilitating the virus entry and to proteins responsible for the virus release (Boopathi et al., 2020; Lo et al., 2020; Wu C and Zheng M, 2020). Several in silico and in vivo drug repurposing studies are carried out using proteases (3CL^{pro} and PL^{pro}) and RNA-dependent RNA polymerase (RdRp) of SARS-CoV-2 as targets (Bharadwaj et al., 2020; Ghosh et al., 2020; Gul et al., 2020; Li et al., 2020c; Wang, 2020). In addition, host proteins TMPRSS2 and ACE2 which primes protein S and mediates SARS-CoV-2 entry to host, respectively, are targeted for drug repositioning as well (Bagheri and Niavarani, 2020; Busnadiego et al., 2020; Carino et al., 2020; Choudhary et al., 2020; Durdagi, 2020; Kumar et al., 2020; Singh et al., 2020b).

NRP1 is a recently identified receptor that facilitates the SARS-CoV-2 cell entry in coordination with ACE2 and TMPRSS2 (Cantuti-Castelvetri et al., 2020; Daly et al., 2020). S protein of SARS-CoV-2 attaches to the host cells for the virus entry (Wang et al., 2020; Yan et al., 2020). When the S protein is cleaved by the host protease, S1 and S2 proteins are generated. S1 has a polybasic sequence (Arg^{682}-Arg-Ala-Arg^{685}) at the C-terminal which interacts with b1 domain of NRP1 (Cantuti-Castelvetri et al., 2020; Daly et al., 2020) (Figure 1). Mutating the critical Arg^{685} diminishes protein S and NRP1 binding (Daly et al., 2020) and antibody against b1b2 domain of NRP1 relieve the SARS-CoV-2 infection (Cantuti-Castelvetri et al., 2020). Drugs having a high affinity to CendR binding pocket of NRP1 can be used in the COVID-19 treatment by blocking SARS-CoV-2 entry into cells.

3.1. Docking simulations

AutoDock Vina program was used to calculate binding energy and predict the binding mode of drugs to the target pocket as described before (Gul et al., 2020; Tardu et al., 2016). During the docking simulations, receptor (NRP1) was treated as a rigid body and drugs were allowed to sample different conformations in the CendR binding pocket. NRP1 inhibitor, EG01377 (Powell et al., 2018), was docked to NRP1 as a control to evaluate the binding affinities of drugs against NRP1. Vina binding energy of EG01377 was calculated as -6.0 kcal/mol (Table 1). The docked conformation of EG01377 is in contact with Tyr[297], Trp[301], Lys[351], and Tyr[353] similar to observed in the crystal structure (PDB ID: 6fmc) (Figure 2A). Docking simulations revealed that over 100 molecules have Vina binding energies -7.6 kcal/mol or lower (Table S1). Histogram representation of Vina binding energies of all drugs are provided in (Figure S1). Top 15 of those drugs having the Vina binding energies between -8.5 and -8.0 kcal/mol were given in (Table 1) with their ZINC IDs, structures, and types.

Docking simulations showed that, according to the descriptions in DrugBank (Wishart et al., 2006), various types of drugs such as anticancer, antipsychotics, anti-inflammatory, antibiotics, antidiabetics, and estrogen hormone may bind to NRP1 (Table S1). For further analysis, widely used drugs eltrombopag (-8.5 kcal/mol), glimepiride (-8.2 kcal/mol), dutasteride (-8.2 kcal/mol), sitagliptin (-8.2 kcal/mol), ergotamine (-8.1 kcal/mol) at the top of the docking result list, and two anti-malarial drugs, mefloquine (-8.0 kcal/mol) and atovaquone (-7.9 kcal/mol), having similar binding energies to top drugs were selected. The binding poses of selected drugs occupy the pocket surrounded by Tyr[297], Trp[301], Lys[351], and Tyr[353] in docking simulations which supports the idea of these drugs may behave as NRP1 inhibitors (Figure 2B,C). To evaluate the persistency

and strength of drug-NRP1 complexes near physiological conditions, MD simulations were run.

3.2.   MD Simulations and Binding Free Energy Calculation

In short MD simulations (20 ns) eltrombopag, glimepiride, dutasteride, sitagliptin, and ergotamine stably interacted with NRP1, however, atovaquone and mefloquine did not. These two antimalarial drugs left their initial docking positions and moved to the solution even in two independent trials. Then I extended 20 ns simulations for those who could interact with the protein in these short simulations to 100 ns to assess the stability of their interaction with NRP1. In a control simulation, the EG01377-NRP1 complex obtained from the docking was simulated for 100 ns. Visual inspection of long simulations showed that all selected drugs and the inhibitor retained their docking positions on the NRP1 through the entire simulation. Root mean square deviation analysis (RMSD) of C_α atoms showed that simulations reached equilibrium around 2Å after an initial jump within 1-2 ns (Figure 3).

To examine the interaction between drugs and critical residues I visualized the contact frequency between drugs and selected amino acids around the binding pocket. Thus, the persistency of drug-amino acid interactions observed in the initial docking position could be assessed (Figure 4A-F). Docking of EG01377 showed that the inhibitor interacts with Tyr^{297}, Trp^{301}, Thr^{316}, Glu^{348}, Thr^{349}, Lys^{351}, Trp^{353}. In MD simulations, EG01377 interacted frequently with Tyr^{297}, Trp^{301}, Thr^{316}, and Tyr^{353} which have aromatic (Tyr and Trp) and polar (Thr) side chains. In addition to these highly interacting amino acids, the inhibitor interacted with Glu^{348} and Thr^{349} through 100 ns simulation (Figure 4A). As a result, MD simulation of EG01377-NRP1 analysis verified interacting residues in the

docking. Frequency analysis for eltrombopag-NRP1 simulation indicated that similar to EG01377, Tyr[297], Trp[301], Thr[316], and Tyr[353] are the frequently interacting residues. The same residues were also identified in docking simulation (Figure 4B). One minor difference between EG01377 and eltrombopag simulations is that while EG01377 interacted with Gly[318], eltrombopag interacted more with Gly[414].

Glimepiride and sitagliptin frequently interacted with the same amino acids that are Tyr[297], Trp[301], Thr[316], Thr[349], and Tyr[353] (Figure 4C, E) in MD simulations. Since binding pocket amino acids are mainly hydrophobic some interactions altered throughout the simulations. For example, interaction with highly interacting amino acids Thr[349] and Lys[351] fluctuated as simulations progressed. Despite slight differences in their docking positions, interacting residues in docking simulations are very similar. While glimepiride interacted with Tyr[297], Trp[301], Thr[316], Glu[348], Thr[349], and Tyr[353], sitagliptin fitted a deeper part of the pocket and, in addition to glimepiride's interacting amino acids, interacted with Thr[316] (Figure 4C, E). Overall, nearby residues observed in docking simulations of glimepiride and sitagliptin were verified by MD simulations.

The docking position of dutasteride showed that the drug interacts with Tyr[297], Thr[349], Lys[351], and Tyr[353]. MD simulation of dutasteride-NRP1 showed that dutasteride behaved less similarly with the inhibitor and did not interact with Trp[301] and Tyr[353] after a certain time (Figure 4D). Possibly dutasteride translated in the binding pocket and started to interact with new residues such as Gly[318], Glu[319], Asp[320], and Ile[415].

Ergotamine showed similar interaction frequency patterns with the inhibitor and constantly interacted with Tyr[297], Trp[301], Thr[316], and Tyr[353] (Figure 4F). In addition to these, ergotamine interacted with Asp[320], Thr[349], and Ile[415] in certain periods of the MD simulation. In docking simulation ergotamine interacted with Tyr[297], Trp[301], Thr[316],

Ser[346], Glu[348], Thr[349], Lys[351], and Tyr[353]. While some of the amino acids recognized in the docking lost contact with ergotamine such as Ser[346] and Glu[348], most of them interacted with ergotamine in the whole MD simulation.

To determine the binding free energy (BFE) between drugs and NRP1 I used MM/GBSA method. The BFE of eltrombopag, glimepiride, dutasteride, sitagliptin, and ergotamine was calculated as -17.11, -12.55, -9.47, -13.34, and -14.95 kcal/mol, respectively (Table 2). BFE of EG01377 was calculated as -16.19 kcal/mol.

A well-tolerated drug eltrombopag stimulates platelet synthesis in patients having low blood platelet (Erickson-Miller et al., 2009). In comparison to EG01377, eltrombopag has better Vina binding energy (-8.5 kcal/mol) and BFE (-17.11 kcal/mol) calculated from docking and MD simulations, respectively. During the MD simulations interacting residues of EG01377 and eltrombopag with NRP1 are very similar to each other (Figure 4B). A previous drug-repurposing study against 3CL[pro] and RdRp of SARS-CoV-2 from our group showed that eltrombopag may bind to the active site of 3CL[pro] and nsp8 binding site of RdRp which may attenuate the virus activity (Gul et al., 2020). Eltrombopag exhibits in vitro antiviral properties with IC_{50} lower than 10µM (Jeon et al., 2020). This report shows that eltrombopag can strongly interact with NRP1, too. If these in silico findings can be verified by in vitro and cell-culture experiments, eltrombopag can be a very strong anti-viral drug by blocking SARS-CoV-2-NRP1 binding to host and alleviating the virus replication.

Two antidiabetics, glimepiride and sitagliptin are well-tolerated drugs used to treat type2 diabetes (Bautista et al., 2003; Raz et al., 2008). Both drugs have the same Vina binding energies (-8.2 kcal) in docking simulations and very similar BFEs calculated from MM/GBSA analysis that are -13.34 and -12.55 kcal/mol for sitagliptin and glimepiride,

respectively. Interacting amino acid residues and BFEs of these antidiabetics are quite alike to EG01377 (Figure 4C, E). Sitagliptin is an inhibitor of dipeptidyl-peptidase IV (DPP-4) that is the host receptor of the Middle East respiratory syndrome (MERS)-CoV (Karasik et al., 2008; Raj et al., 2013) and *in silico* studies suggested that protein S of SARS-CoV-2 can bind to DPP4 as well (Li et al., 2020b; Vankadari and Wilce, 2020). Administration of sitagliptin to patients suffering from diabetes and COVID-19 does not only help to lower the blood glucose level but may also reduce the SARS-CoV-2 entry to the cells.

Dutasteride, another well-tolerated drug, inhibits type I and II 5α-reductase and shows anti-androgenic activity (Andriole and Kirby, 2003; Roehrborn et al., 2002). 5α-reductase converts testosterone to dihydrotestosterone and enlarges the prostate glands. Thus, dutasteride is used to treat prostatic conditions by blocking the 5α-reductase activity (Makridakis et al., 2000). Besides the effect on the prostate gland, dutasteride suppresses the transmembrane serine protease 2 (TMPRSS2) expression (Mostaghel et al., 2014) which primes protein S of the SARS-CoV-2 (Hoffmann et al., 2020b). Docking binding energy and MM/GBSA calculations show that dutasteride has a high affinity to NRP1 (Table1, 2). Relatively higher BFE with a high standard deviation of dutasteride-NRP1 may stem from the loss of interaction between dutasteride and two aromatic residues Trp^{301} and Tyr^{353} as shown in frequency analysis (Figure 4(D)). However, dutasteride has still a high affinity to the NRP1 and interacts with amino acids observed in docking simulations. Despite further in vivo analysis needed, dutasteride may be a preventive drug that shuts down the virus entry by blocking the NRP1 and downregulating the TMPRSS2. Antimigraine ergotamine is a tolerable drug with mild and transient side effects (Christie et al., 2003; Diener et al., 2002). Several *in silico* drug repurposing studies reported that

ergotamine may inhibit the RdRp and 3CL^{pro} of SARS-CoV-2 (Barage et al., 2020; Gul et al., 2020). Ergotamine has the second-best BFE among all drugs analyzed in this study (Table 2). Comparable BFEs of ergotamine and EG01377 to NRP1 suggests that ergotamine can strongly bind to NRP1, in turn, can attenuate NRP1-protein S binding. If these computational analyses can be experimentally verified, ergotamine can be used to mitigate the COVID-19. To note, it has been reported that ergotamine may cross-react with antiviral drugs (Ayarragaray, 2014; Mortier et al., 2001; Rosenthal et al., 1999). Thus, further studies related to ergotamine should be designed accordingly.

Comparable BFE and interaction pattern of inhibitor and selected drugs indicate that these drugs may act as NRP1 inhibitors.

3.3. H-bond and Ala-Scanning Analysis

To describe the type of interactions drug made during the MD simulation I analyzed the hydrogen bond (H-bond) generated by drugs to any amino acids through 100 ns (Figure 5). Calculation of the average number of H-bonds showed that each drug, including the inhibitor, produced less than one H-bond per frame. These results indicated that interactions between drugs and the protein are mostly hydrophobic.

To reveal the critical amino acids for drug binding and quantify their contribution to BFE, I performed in silico Alanine scanning mutation. The most frequently and commonly interacting amino acids e.g. Tyr^{297}, Trp^{301}, Thr^{316}, and Tyr^{353} in all drug/inhibitor-NRP1 simulations were analyzed (Figure 4 A-F). These residues were mutated to Alanine one by one and BFE between drugs and NRP1 was calculated using the MM/GBSA method (Table 3). Then the difference between BFEs of drugs against mutant and wild-type NRP1 is calculated ($\Delta\Delta G$). $\Delta\Delta G$ values larger than 0 means that mutation is destabilizing the

interaction, ΔΔG lower than 0 means mutation is stabilizing the interaction. According to ΔΔG values, Tyr^{297}, Trp^{301}, and Tyr^{353} are very critical for all drugs binding to NRP1. Interestingly, despite high interaction with drugs, Thr^{316} minimally contributes to BFE. Individually, Tyr^{297} is critical for EG01377, eltrombopag, and dutasteride; Trp^{301} is critical for ergotamine; Tyr^{353} is critical for sitagliptin and glimepiride binding to NRP1(Table 3). The contribution of each mutated amino acid to drug-NRP1 BFE is given (Figure 6).

H-bond and Ala-scanning calculations provide a deeper understanding of drug-NRP1 interactions. Future structure-activity relationship (SAR) studies aim to design a more potent NRP1 inhibitor may benefit from the critical amino acids identified here. Adding an H-bond donor or acceptor to a new molecule can increase the binding affinity to NRP1.

4.   Conclusion

ADespite substantial progress has been made by several companies for the SARS-CoV-2 vaccine (Corbett et al., 2020; Mulligan et al., 2020; Sahin et al., 2020) only several governments approved for emergency use authorization. So, medication is still an essential element to combat COVID-19. Vital enzymes of SARS-CoV-2 such as proteases (3CL^{pro} and M^{pro}) and RNA polymerase (RdRp), or virus binding receptors on the host such as ACE2 or TMPRSS2 are generally targeted in drug repurposing studies (Bagheri and Niavarani, 2020; Busnadiego et al., 2020; Carino et al., 2020; Gul et al., 2020; Kumar et al., 2020; Li et al., 2020c; Singh et al., 2020b). Recent studies reported protein S binds to NRP1 which facilitates SARS-CoV-2 host entry (Cantuti-Castelvetri et al., 2020; Daly et al., 2020). Here a drug repurposing study was done against NRP1 in terms of docking and MD simulations using the FDA approved drugs. Furthermore, key amino acids on NRP1 for drug binding were identified by running Ala-scanning analysis. Several well-tolerated drugs showed comparable and even better affinity to NRP1 than its inhibitor EG01377. Eltrombopag had the best binding affinity to NRP1 among all drugs. In addition to eltrombopag, two antidiabetics, sitagliptin and glimepiride stably interacted with and exhibited high affinity to NRP1. Since patients having chronic diseases such as diabetes are at more risk against COVID-19, those suffering from diabetes may benefit from sitagliptin and glimepiride not only as antidiabetics but also their preventive effects, if proven by experiment, against SARS-CoV-2 infection. Dutasteride may provide multiple benefits to COVID-19 patients. First, it reduces the expression of TMPRSS2 that primes the S-protein (Hoffmann et al., 2020a; Hoffmann et al., 2020b). Two, in silico studies reported that it may block 3CL^{pro} (Gul et al., 2020). Third, this study shows that dutasteride can bind to and strongly interact with NRP1, thus, may decrease SARS-CoV-

2 entry. Ergotamine is another top candidate molecule for the NRP1 binding. Previous calculations showed that ergotamine has the potential to bind to 3CL^{pro} and RdRp of SARS-CoV-2 (Gul et al., 2020; Rahman et al., 2020). So, ergotamine may inhibit SARS-CoV-2 at the infection and replication stages. H-bond analysis showed that drugs have a few numbers of H-bond interactions with NRP1. Ala-scanning calculations uncovered that Tyr^{297}, Trp^{301}, and Tyr^{353} are the most critical amino acid residues for drug binding to NRP1. H-bond analysis and Ala-scanning results may be exploited by further inhibitor design studies.

To expedite the discovery of therapeutics for COVID-19 drug repurposing studies may provide a rational starting point. If the findings of this study can be verified by in vitro, in vivo, and clinical trials these well-tolerated and cost-effective drugs can be adapted to current protocols used to treat COVID-19.

References

Andriole, G.L., and Kirby, R. (2003). Safety and tolerability of the dual 5 alpha-reductase inhibitor dutasteride in the treatment of benign prostatic hyperplasia. European Urology *44*, 82-88.

Ayarragaray, J.E.F. (2014). Ergotism: A Change of Persepective. Annals of Vascular Surgery *28*, 265-268.

Baez-Santos, Y.M., St John, S.E., and Mesecar, A.D. (2015). The SARS-coronavirus papain-like protease: Structure, function and inhibition by designed antiviral compounds. Antiviral Research *115*, 21-38.

Bagheri, M., and Niavarani, A. (2020). Molecular dynamics analysis predicts ritonavir and naloxegol strongly block the SARS-CoV-2 spike protein-hACE2 binding. Journal of Biomolecular Structure & Dynamics.

Barage, S., Karthic, A., Bavi, R., Desai, N., Kumar, R.*, et al.* (2020). Identification and characterization of novel RdRp and Nsp15 inhibitors for SARS-COV2 using computational approach. Journal of Biomolecular Structure & Dynamics.

Bautista, J.L., Bugos, C., Dirnberger, G., and Atherton, T. (2003). Efficacy and safety profile of glimepiride in Mexican American patients with type 2 diabetes mellitus: A randomized, placebo-controlled study. Clinical Therapeutics *25*, 194-209.

Bharadwaj, S., Azhar, E.I., Kamal, M.A., Bajrai, L.H., Dubey, A.*, et al.* (2020). SARS-CoV-2 M-pro inhibitors: identification of anti-SARS-CoV-2 M-pro compounds from FDA approved drugs. Journal of Biomolecular Structure & Dynamics.

Boopathi, S., Poma, A.B., and Kolandaivel, P. (2020). Novel 2019 coronavirus structure, mechanism of action, antiviral drug promises and rule out against its treatment. J Biomol Struct Dyn, 1-10.

Busnadiego, I., Fernbach, S., Pohl, M.O., Karakus, U., Huber, M.*, et al.* (2020). Antiviral Activity of Type I, II, and III Interferons Counterbalances ACE2 Inducibility and Restricts SARS-CoV-2. Mbio *11*.

Cantuti-Castelvetri, L., Ojha, R., Pedro, L.D., Djannatian, M., Franz, J.*, et al.* (2020). Neuropilin-1 facilitates SARS-CoV-2 cell entry and infectivity. Science, eabd2985.

Cao, S., Yaqoob, U., Das, A., Shergill, U., Jagavelu, K.*, et al.* (2010). Neuropilin-1 promotes cirrhosis of the rodent and human liver by enhancing PDGF/TGF-beta signaling in hepatic stellate cells. Journal of Clinical Investigation *120*, 2379-2394.

Carino, A., Moraca, F., Fiorillo, B., Marchiano, S., Sepe, V.*, et al.* (2020). Hijacking SARS-CoV-2/ACE2 Receptor Interaction by Natural and Semi-synthetic Steroidal Agents Acting on Functional Pockets on the Receptor Binding Domain. Frontiers in Chemistry *8*.

Case, D.A., Belfon, K., Ben-Shalom, I.Y., Brozell, S.R., Cerutti, D.S.*, et al.* (2020). AMBER 2020 (University of California, San Francisco).

Choudhary, S., Malik, Y.S., and Tomar, S. (2020). Identification of SARS-CoV-2 Cell Entry Inhibitors by Drug Repurposing Usingin silicoStructure-Based Virtual Screening Approach. Frontiers in Immunology *11*.

Christie, S., Gobel, H., Mateos, V., Allen, C., Vrijens, F.*, et al.* (2003). Crossover comparison of efficacy and preference for rizatriptan 10 mg versus ergotamine/caffeine in migraine. European Neurology *49*, 20-29.

Corbett, K.S., Flynn, B., Foulds, K.E., Francica, J.R., Boyoglu-Barnum, S.*, et al.* (2020). Evaluation of the mRNA-1273 Vaccine against SARS-CoV-2 in Nonhuman Primates. New England Journal of Medicine *383*, 1544-1555.

Daly, J.L., Simonetti, B., Klein, K., Chen, K.-E., Williamson, M.K.*, et al.* (2020). Neuropilin-1 is a host factor for SARS-CoV-2 infection. Science, eabd3072.

DeLano, W.L. (2009). PyMOL molecular viewer: Updates and refinements. Abstracts of Papers of the American Chemical Society *238*.

Diener, H.C., Jansen, J.P., Reches, A., Pascual, J., Pitei, D.*, et al.* (2002). Efficacy, tolerability and safety of oral eletriptan and ergotamine plus caffeine (Cafergot (R)) in the acute treatment of migraine: A multicentre, randomised, double-blind, placebo-controlled comparison. European Neurology *47*, 99-107.

Donoghue, M., Hsieh, F., Baronas, E., Godbout, K., Gosselin, M.*, et al.* (2000). A Novel Angiotensin-Converting Enzyme–Related Carboxypeptidase (ACE2) Converts Angiotensin I to Angiotensin 1-9. Circulation Research *87*, e1-e9.

Doruk, Y.U., Yarparvar, D., Akyel, Y.K., Gul, S., Taskin, A.C.*, et al.* (2020). A CLOCK-binding small molecule disrupts the interaction between CLOCK and BMAL1 and enhances circadian rhythm amplitude. Journal of Biological Chemistry *295*, 3518-3531.

Du, Q.S., Wang, S.Q., Zhu, Y., Wei, D.Q., Guo, H.*, et al.* (2004). Polyprotein cleavage mechanism of SARS CoV M-pro and chemical modification of the octapeptide. Peptides *25*, 1857-1864.

Durdagi, S. (2020). Virtual drug repurposing study against SARS-CoV-2 TMPRSS2 target. Turkish Journal of Biology *44*, 185-+.

Erickson-Miller, C.L., Delorme, E., Tian, S.S., Hopson, C.B., Landis, A.J.*, et al.* (2009). Preclinical activity of eltrombopag (SB-497115), an oral, nonpeptide thrombopoietin receptor agonist. Stem Cells *27*, 424-430.

Fantin, A., Herzog, B., Mahmoud, M., Yamaji, M., Plein, A.*, et al.* (2014). Neuropilin 1 (NRP1) hypomorphism combined with defective VEGF-A binding reveals novel roles for NRP1 in developmental and pathological angiogenesis. Development *141*, 556-562.

Ghosh, R., Chakraborty, A., Biswas, A., and Chowdhuri, S. (2020). Potential therapeutic use of corticosteroids as SARS CoV-2 main protease inhibitors: a computational study. Journal of Biomolecular Structure & Dynamics.

Gul, S., Ozcan, O., Asar, S., Okyar, A., Baris, I.*, et al.* (2020). In silico identification of widely used and well-tolerated drugs as potential SARS-CoV-2 3C-like protease and viral RNA-dependent RNA polymerase inhibitors for direct use in clinical trials. Journal of Biomolecular Structure & Dynamics.

Hoffmann, M., Kleine-Weber, H., and Pohlmann, S. (2020a). A Multibasic Cleavage Site in the Spike Protein of SARS-CoV-2 Is Essential for Infection of Human Lung Cells. Molecular Cell *78*, 779-+.

Hoffmann, M., Kleine-Weber, H., Schroeder, S., Kruger, N., Herrler, T.*, et al.* (2020b). SARS-CoV-2 Cell Entry Depends on ACE2 and TMPRSS2 and Is Blocked by a Clinically Proven Protease Inhibitor. Cell *181*, 271-+.

Huang, J., Rauscher, S., Nawrocki, G., Ran, T., Feig, M.*, et al.* (2017). CHARMM36m: an improved force field for folded and intrinsically disordered proteins. Nat Methods *14*, 71-73.

Humphrey, W., Dalke, A., and Schulten, K. (1996). VMD: visual molecular dynamics. J Mol Graph *14*, 33-38, 27-38.

Jarvis, A., Allerston, C.K., Jia, H.Y., Herzog, B., Garza-Garcia, A.*, et al.* (2010). Small Molecule Inhibitors of the Neuropilin-1 Vascular Endothelial Growth Factor A (VEGF-A) Interaction. Journal of Medicinal Chemistry *53*, 2215-2226.

Jeon, S., Ko, M., Lee, j., Choi, I., Young Byun, S.*, et al.* (2020). Identification of antiviral drug candidates against SARS-CoV-2 from FDA-approved drugs. https://doiorg/101101/20200320999730.

Jia, H.Y., Aqil, R., Cheng, L.L., Chapman, C., Shaikh, S.*, et al.* (2014). N-Terminal Modification of VEGF-A C Terminus-Derived Peptides Delineates Structural Features Involved in Neuropilin-1 Binding and Functional Activity. Chembiochem *15*, 1161-1170.

Jo, S., Kim, T., Iyer, V.G., and Im, W. (2008). CHARMM-GUI: a web-based graphical user interface for CHARMM. J Comput Chem *29*, 1859-1865.

Karasik, A., Aschner, P., Katzeff, H., Davies, M.J., and Stein, P.P. (2008). Sitagliptin, a DPP-4 inhibitor for the treatment of patients with type 2 diabetes: a review of recent clinical trials. Current Medical Research and Opinion *24*, 489-496.

Kim, S., Lee, J., Jo, S., Brooks, C.L., 3rd, Lee, H.S.*, et al.* (2017). CHARMM-GUI ligand reader and modeler for CHARMM force field generation of small molecules. J Comput Chem *38*, 1879-1886.

Kumar, V., Dhanjal, J.K., Bhargava, P., Kaul, A., Wang, J.*, et al.* (2020). Withanone and Withaferin-A are predicted to interact with transmembrane protease serine 2 (TMPRSS2) and block entry of SARS-CoV-2 into cells. Journal of Biomolecular Structure & Dynamics.

Li, H., Zhou, Y., Zhang, M., Wang, H., Zhao, Q.*, et al.* (2020a). Updated approaches against SARS-CoV-2. Antimicrob Agents Chemother.

Li, Y., Zhang, Z.D., Yang, L., Lian, X.Y., Xie, Y.*, et al.* (2020b). The MERS-CoV Receptor DPP4 as a Candidate Binding Target of the SARS-CoV-2 Spike. Iscience *23*.

Li, Z., Li, X., Huang, Y.Y., Wu, Y.X., Liu, R.D.*, et al.* (2020c). Identify potent SARS-CoV-2 main protease inhibitors via accelerated free energy perturbation-based virtual screening of existing drugs. Proceedings of the National Academy of Sciences of the United States of America *117*, 27381-27387.

Liu, Y., Mao, B., Liang, S., Yang, J.W., Lu, H.W.*, et al.* (2020). Association between age and clinical characteristics and outcomes of COVID-19. European Respiratory Journal *55*.

Lo, H.S., Hui, K.P.Y., Lai, H.-M., Khan, K.S., Kaur, S.*, et al.* (2020). Simeprevir suppresses SARS-CoV-2 replication and synergizes with remdesivir. bioRxiv, DOI:101101/20200526116020.

Makridakis, N.M., di Salle, E., and Reichardt, J.K.V. (2000). Biochemical and pharmacogenetic dissection of human steroid 5 alpha-reductase type II. Pharmacogenetics *10*, 407-413.

Mortier, E., Pouchot, J., Vinceneux, P., and Lalande, M. (2001). Ergotism related to interaction between nelfinavir and ergotamine. American Journal of Medicine *110*, 594-594.

Mostaghel, E.A., Nelson, P.S., Lange, P., Lin, D.W., Taplin, M.E.*, et al.* (2014). Targeted Androgen Pathway Suppression in Localized Prostate Cancer: A Pilot Study. Journal of Clinical Oncology *32*, 229-+.

Mota, F., Fotinou, C., Rana, R.R., Chan, A.W.E., Yelland, T.*, et al.* (2018). Architecture and hydration of the arginine-binding site of neuropilin-1. Febs Journal *285*, 1290-1304.

Mulligan, M.J., Lyke, K.E., Kitchin, N., Absalon, J., Gurtman, A.*, et al.* (2020). Phase I/II study of COVID-19 RNA vaccine BNT162b1 in adults. Nature *586*, 589-+.

Muramatsu, T., Kim, Y.T., Nishii, W., Terada, T., Shirouzu, M.*, et al.* (2013). Autoprocessing mechanism of severe acute respiratory syndrome coronavirus3C-like protease (SARS-CoV 3CLpro) from its polyproteins. Febs Journal *280*, 2002-2013.

Omori, R., Matsuyama, R., and Nakata, Y. (2020). The age distribution of mortality from novel coronavirus disease (COVID-19) suggests no large difference of susceptibility by age. Scientific Reports *10*, 16642.

Parker, M.W., Xu, P., Li, X.B., and Vander Kooi, C.W. (2012). Structural Basis for Selective Vascular Endothelial Growth Factor-A (VEGF-A) Binding to Neuropilin-1. Journal of Biological Chemistry *287*, 11082-11089.

Phillips, J.C., Braun, R., Wang, W., Gumbart, J., Tajkhorshid, E.*, et al.* (2005). Scalable molecular dynamics with NAMD. J Comput Chem *26*, 1781-1802.

Powell, J., Mota, F., Steadman, D., Soudy, C., Miyauchi, J.T.*, et al.* (2018). Small Molecule Neuropilin-1 Antagonists Combine Antiangiogenic and Antitumor Activity with Immune Modulation through Reduction of Transforming Growth Factor Beta (TGF beta) Production in Regulatory T-Cells. Journal of Medicinal Chemistry *61*, 4135-4154.

Rahman, M.M., Saha, T., Islam, K.J., Suman, R.H., Biswas, S.*, et al.* (2020). Virtual screening, molecular dynamics and structure-activity relationship studies to identify potent approved drugs for Covid-19 treatment. Journal of Biomolecular Structure & Dynamics.

Raj, V.S., Mou, H.H., Smits, S.L., Dekkers, D.H.W., Muller, M.A.*, et al.* (2013). Dipeptidyl peptidase 4 is a functional receptor for the emerging human coronavirus-EMC. Nature *495*, 251-254.

Raz, I., Chen, Y., Wu, M., Hussain, S., Kaufman, K.D.*, et al.* (2008). Efficacy and safety of sitagliptin added to ongoing metformin therapy in patients with type 2 diabetes. Current Medical Research and Opinion *24*, 537-550.

Roehrborn, C.G., Boyle, P., Nickel, J.C., Hoefner, K., Andriole, G.*, et al.* (2002). Efficacy and safety of a dual inhibitor of 5-alpha-reductase types 1 and 2 (dutasteride) in men with benign prostatic hyperplasia. Urology *60*, 434-441.

Rosenthal, E., Sala, F., Chichmanian, R.M., Batt, M., and Cassuto, J.P. (1999). Ergotism related to concurrent administration of ergotamine tartrate and indinavir. JAMA *281*, 987.

Sahin, U., Muik, A., Derhovanessian, E., Vogler, I., Kranz, L.M.*, et al.* (2020). COVID-19 vaccine BNT162b1 elicits human antibody and T(H)1T cell responses. Nature *586*, 594-+.

Sarma, P., Shekhar, N., Prajapat, M., Avti, P., Kaur, H.*, et al.* (2020). In-silico homology assisted identification of inhibitor of RNA binding against 2019-nCoV N-protein (N terminal domain). J Biomol Struct Dyn, 1-9.

Schoeman, D., and Fielding, B.C. (2019). Coronavirus envelope protein: current knowledge. Virology Journal *16*.

Shang, J., Wan, Y.S., Luo, C.M., Ye, G., Geng, Q.B.*, et al.* (2020). Cell entry mechanisms of SARS-CoV-2. Proceedings of the National Academy of Sciences of the United States of America *117*, 11727-11734.

Singh, K.K., Chaubey, G., Chen, J.Y., and Suravajhala, P. (2020a). Decoding SARS-CoV-2 hijacking of host mitochondria in COVID-19 pathogenesis. American Journal of Physiology-Cell Physiology *319*, C258-C267.

Singh, N., Decroly, E., Khatib, A.M., and Villoutreix, B.O. (2020b). Structure-based drug repositioning over the human TMPRSS2 protease domain: search for chemical probes able to repress SARS-CoV-2 Spike protein cleavages. European Journal of Pharmaceutical Sciences *153*.

Soker, S., Takashima, S., Miao, H.Q., Neufeld, G., and Klagsbrun, M. (1998). Neuropilin-1 is expressed by endothelial and tumor cells as an isoform-specific receptor for vascular endothelial growth factor. Cell *92*, 735-745.

Sulpice, E., Plouet, J., Berge, M., Allanic, D., Tobelem, G.*, et al.* (2008). Neuropilin-1 and neuropilin-2 act as coreceptors, potentiating proangiogenic activity. Blood *111*, 2036-2045.

Tardu, M., Rahim, F., Kavakli, I.H., and Turkay, M. (2016). Milp-Hyperbox Classification for Structure-Based Drug Design in the Discovery of Small Molecule Inhibitors of Sirtuin6. Rairo-Operations Research *50*, 387-400.

Teesalu, T., Sugahara, K.N., Kotamraju, V.R., and Ruoslahti, E. (2009). C-end rule peptides mediate neuropilin-1-dependent cell, vascular, and tissue penetration. Proceedings of the National Academy of Sciences of the United States of America *106*, 16157-16162.

Thiel, V., Ivanov, K.A., Putics, A., Hertzig, T., Schelle, B.*, et al.* (2003). Mechanisms and enzymes involved in SARS coronavirus genome expression. Journal of General Virology *84*, 2305-2315.

Trott, O., and Olson, A.J. (2010). AutoDock Vina: improving the speed and accuracy of docking with a new scoring function, efficient optimization, and multithreading. J Comput Chem *31*, 455-461.

Tse, L.V., Hamilton, A.M., Friling, T., and Whittaker, G.R. (2014). A Novel Activation Mechanism of Avian Influenza Virus H9N2 by Furin. Journal of Virology *88*, 1673-1683.

Vander Kooi, C.W., Jusino, M.A., Perman, B., Neau, D.B., Bellamy, H.D.*, et al.* (2007). Structural basis for ligand and heparin binding to neuropilin B domains. Proceedings of the National Academy of Sciences of the United States of America *104*, 6152-6157.

Vankadari, N., and Wilce, J.A. (2020). Emerging COVID-19 coronavirus: glycan shield and structure prediction of spike glycoprotein and its interaction with human CD26. Emerging Microbes & Infections *9*, 601-604.

Venkatagopalan, P., Daskalova, S.M., Lopez, L.A., Dolezal, K.A., and Hogue, B.G. (2015). Coronavirus envelope (E) protein remains at the site of assembly. Virology *478*, 75-85.

Walls, A.C., Park, Y.J., Tortorici, M.A., Wall, A., McGuire, A.T.*, et al.* (2020). Structure, Function, and Antigenicity of the SARS-CoV-2 Spike Glycoprotein. Cell *181*, 281-+.

Wang, J.M. (2020). Fast Identification of Possible Drug Treatment of Coronavirus Disease-19 (COVID-19) through Computational Drug Repurposing Study. Journal of Chemical Information and Modeling *60*, 3277-3286.

Wang, Q.H., Zhang, Y.F., Wu, L.L., Niu, S., Song, C.L.*, et al.* (2020). Structural and Functional Basis of SARS-CoV-2 Entry by Using Human ACE2. Cell *181*, 894-+.

Wishart, D.S., Knox, C., Guo, A.C., Shrivastava, S., Hassanali, M.*, et al.* (2006). DrugBank: a comprehensive resource for in silico drug discovery and exploration. Nucleic Acids Research *34*, D668-D672.

Wolfel, R., Corman, V.M., Guggemos, W., Seilmaier, M., Zange, S.*, et al.* (2020). Virological assessment of hospitalized patients with COVID-2019. Nature.

Wrapp, D., Wang, N.S., Corbett, K.S., Goldsmith, J.A., Hsieh, C.L.*, et al.* (2020). Cryo-EM structure of the 2019-nCoV spike in the prefusion conformation. Science *367*, 1260-+.

Wu, A.P., Peng, Y.S., Huang, B.Y., Ding, X., Wang, X.Y.*, et al.* (2020a). Genome Composition and Divergence of the Novel Coronavirus (2019-nCoV) Originating in China. Cell Host & Microbe *27*, 325-328.

Wu C, L.Y., Yang Y, Zhang P, Zhong W, Wang Y, Wang Q, Xu Y, Li M, Li X,, and Zheng M, C.L., Li H, (2020). Analysis of therapeutic targets for SARS-CoV-2 and discovery of potential drugs

by computational methods. Acta Pharmaceutica Sinica B.

Wu, F., Zhao, S., Yu, B., Chen, Y.M., Wang, W.*, et al.* (2020b). A new coronavirus associated with human respiratory disease in China. Nature.

Yan, R.H., Zhang, Y.Y., Li, Y.N., Xia, L., Guo, Y.Y.*, et al.* (2020). Structural basis for the recognition of SARS-CoV-2 by full-length human ACE2. Science *367*, 1444-+.

Yi, Y., Lagniton, P.N.P., Ye, S., Li, E.Q., and Xu, R.H. (2020). COVID-19: what has been learned and to be learned about the novel coronavirus disease. International Journal of Biological Sciences *16*, 1753-1766.

Yoshimoto, F.K. (2020). The Proteins of Severe Acute Respiratory Syndrome Coronavirus-2 (SARS CoV-2 or n-COV19), the Cause of COVID-19. Protein Journal *39*, 198-216.

Zhang, H., Kang, Z., Gong, H., Xu, D., Wang, J.*, et al.* (2020). The digestive system is a potential route of 2019-nCov infection: a bioinformatics analysis based on single-cell transcriptomes. bioRxiv, 2020.2001.2030.927806.

Zhou, P., Yang, X.L., Wang, X.G., Hu, B., Zhang, L.*, et al.* (2020). A pneumonia outbreak associated with a new coronavirus of probable bat origin. Nature *579*, 270-+.
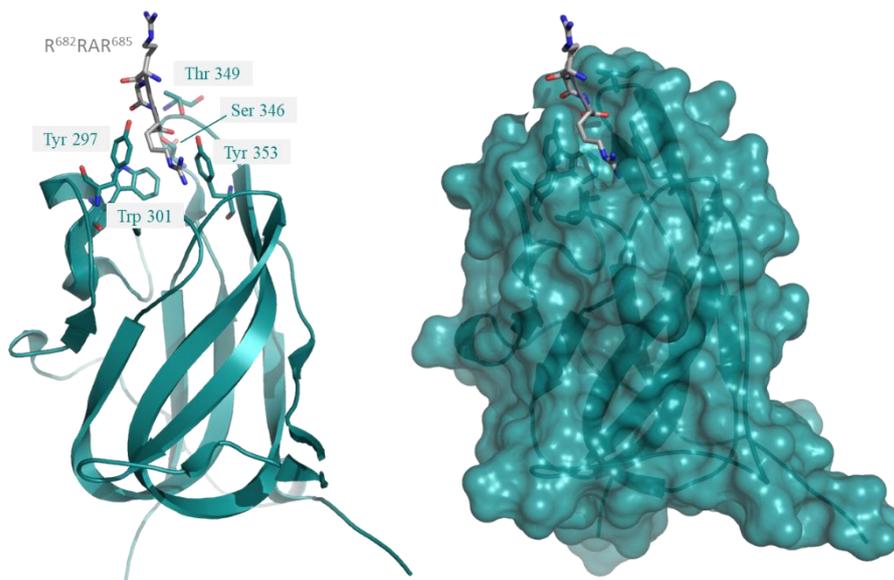
Figure 1. Structure of NRP1 in complex with polybasic peptide at the C-terminal of protein S (PDB ID: 7JJC). NRP1 is shown in cartoon at left critical residues are shown in ball and sticks (cyan color), polybasic peptide is shown in ball and sticks (gray color) representation. NRP1 is shown in surface representation at right.
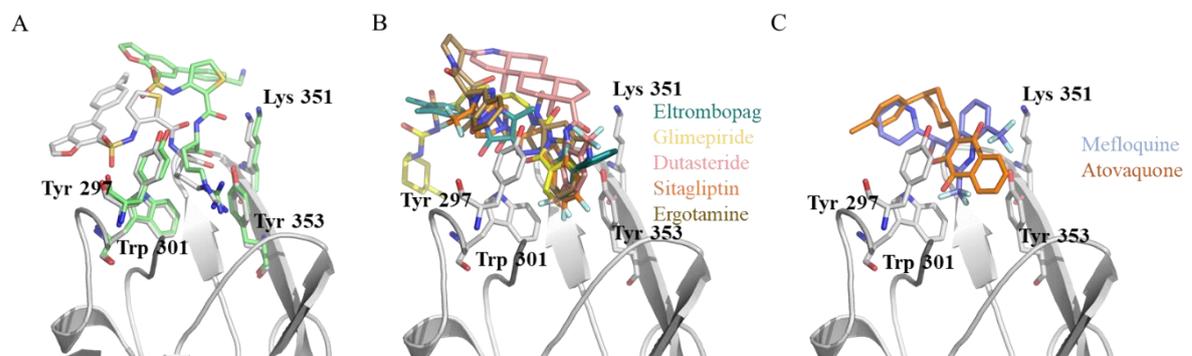
Figure 2. (A) Binding of EG01377 (shown in sticks representation) in the crystal (PDB ID: 6FMC) (carbon atoms are shown in green) in the docking simulation (carbon atoms are shown in white) to b1 domain of NRP1 (shown in white cartoon representation). (B) Binding mode of eltrombopag, glimepiride, dutasteride, sitagliptin, and ergotamine to NRP1 obtained from the docking. (C) Binding of two antimalarial drugs mefloquine and atovaquone to NRP1 obtained from the docking.

Table 1: List of top 15 drugs having the best binding affinity to NRP1 inhibitors.

ZINC ID and/or Drug Name	2D Structure	Vina Binding Affinity (kcal/mol)	Type
ZINC000011679756/ Eltrombopag		-8.5	Thrombopoietin receptor agonist
ZINC000003830767 / Estradiol benzoate		-8.5	Estrogenic steroids
ZINC000064033452 / Lumacaftor		-8.4	Used to treat fibrosis (CF) in patients having homozygous F508del mutation in their CFTR gene.
ZINC000011681563 / Netupitant		-8.3	Antiemetic
ZINC000000006157 / Epinastine		-8.3	Antiallergic
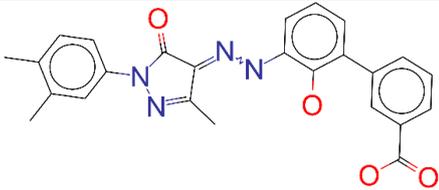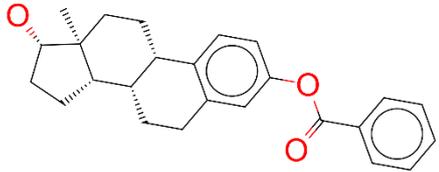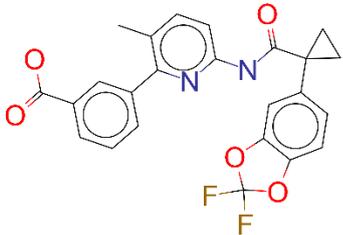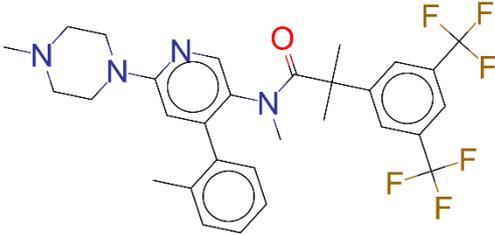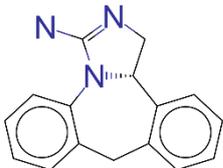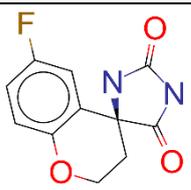
ZINC000000002070 / Sorbinil		-8.3	Inhibitor of aldose reductase
ZINC000000537791 / Glimepiride		-8.2	Antidiabetics
ZINC000003932831 / Dutasteride		-8.2	Antiandrogen
ZINC000001489478 / Sitagliptin		-8.2	Antidiabetics
ZINC000000004724 / Trileptal		-8.2	Anti-epileptic
ZINC000001996117/ Darifenacin		-8.1	Treats urinary incontinence
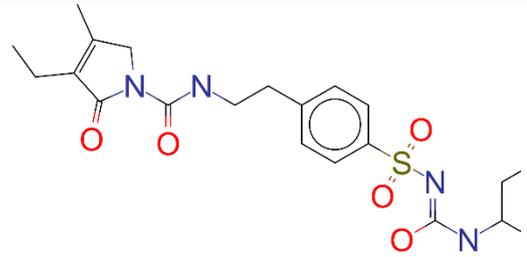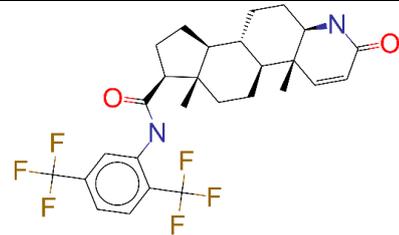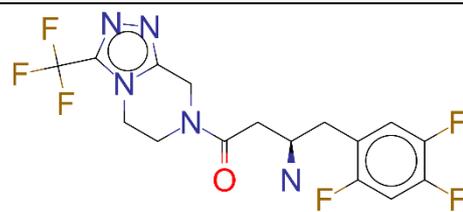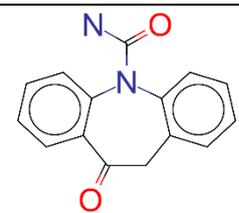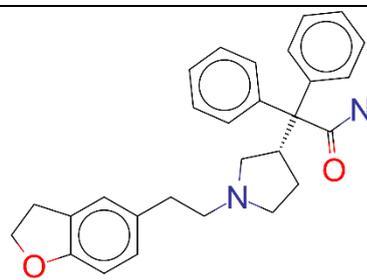
Compound	Structure	Score	Activity
ZINC000052955754 / Ergotamine		-8.1	Antimigraine
ZINC000003831448/ Silibinin		-8.1	Anticancer and various pharmacological effect
ZINC000003978005 / Dihydroergotamine		-8.0	Antimigraine
ZINC000003869855 / Dicumarol		-8.0	Anticoagulant
EG01377		-6.0	Inhibitor of NRP1
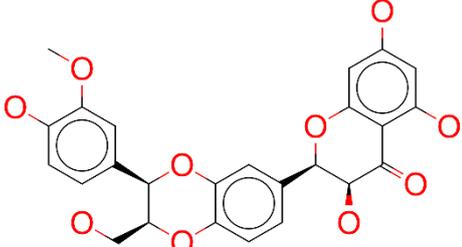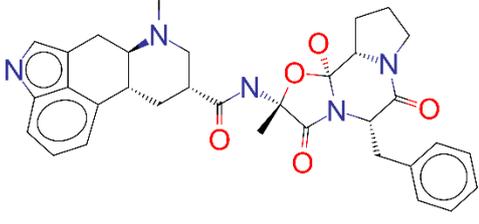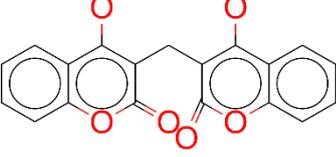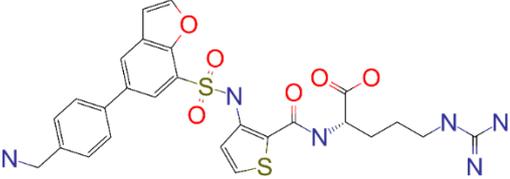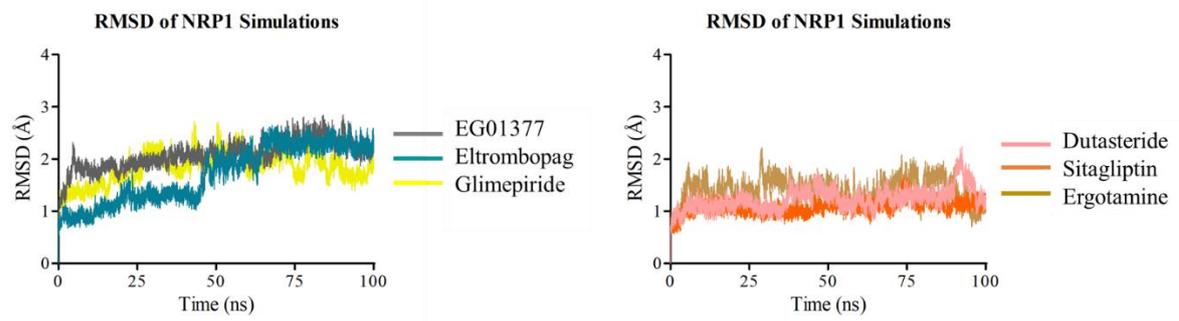
Figure 3. Root mean square deviation (RMSD) of C$_\alpha$ atoms in drug-NRP1 simulations.
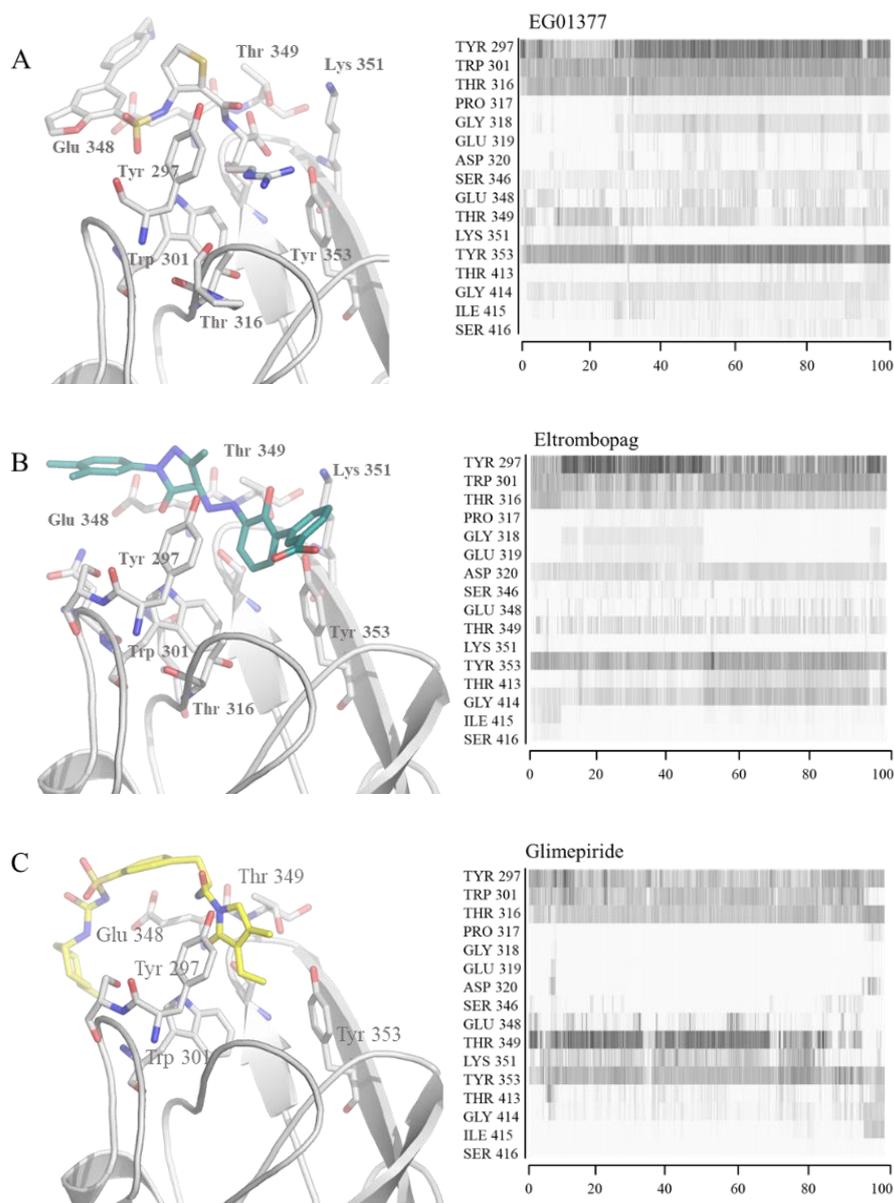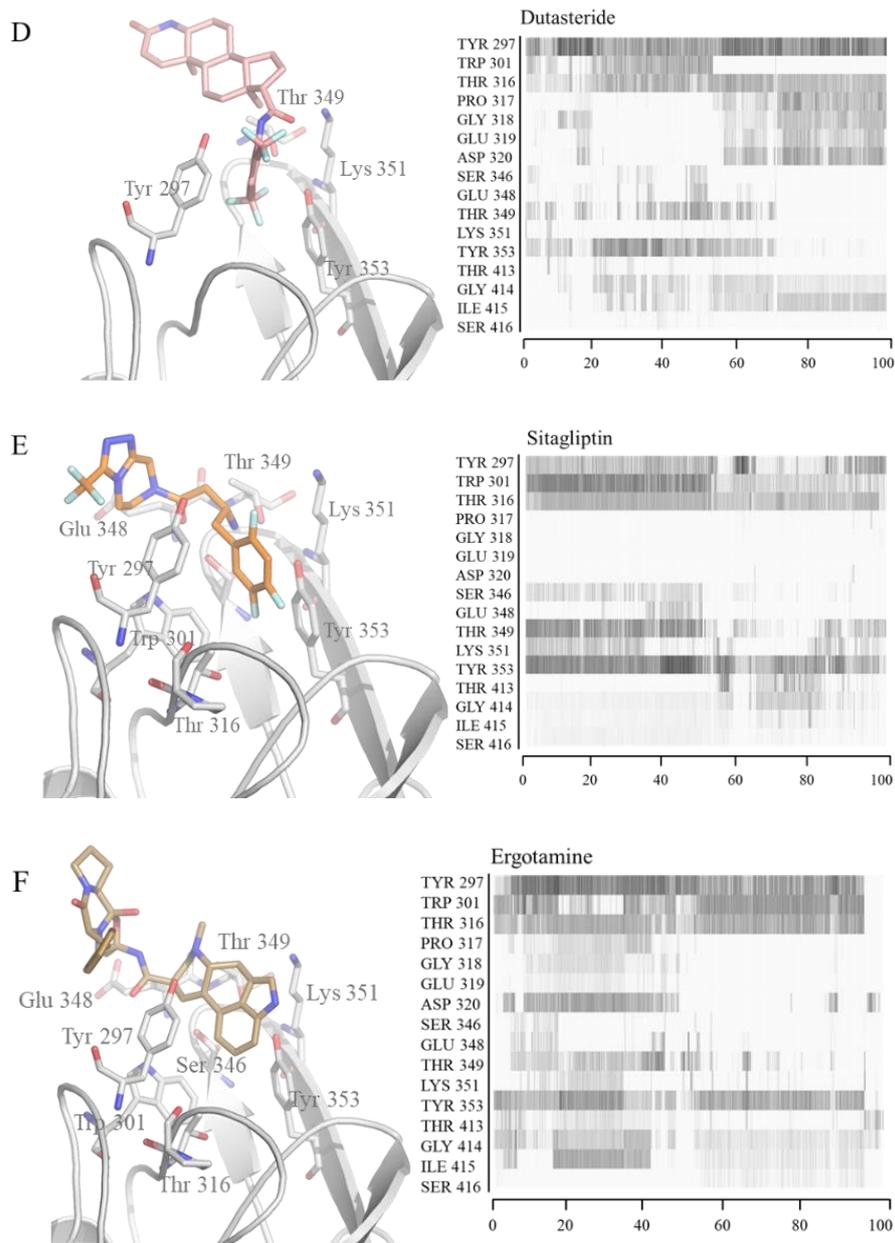
Figure 4. The binding pose in docking simulations and interaction frequency of amino acids from 100 ns MD simulations for NRP1 in complex with (A) EG01377, (B) eltrombopag, (C) glimepiride, (D) dutasteride, (E) sitagliptin, (F) ergotamine

Table 2: MM/GBSA BFE of selected drugs and NRP1 inhibitor

Drug Name	MM/ GBSA BFE (kcal/mol)
Eltrombopag	-17.11±2.99
Ergotamine	14.95±7.40
Sitagliptin	-13.34±3.90
Glimepiride	-12.55±3.48
Dutasteride	9.47±4.41
EG01377	-16.19±4.20
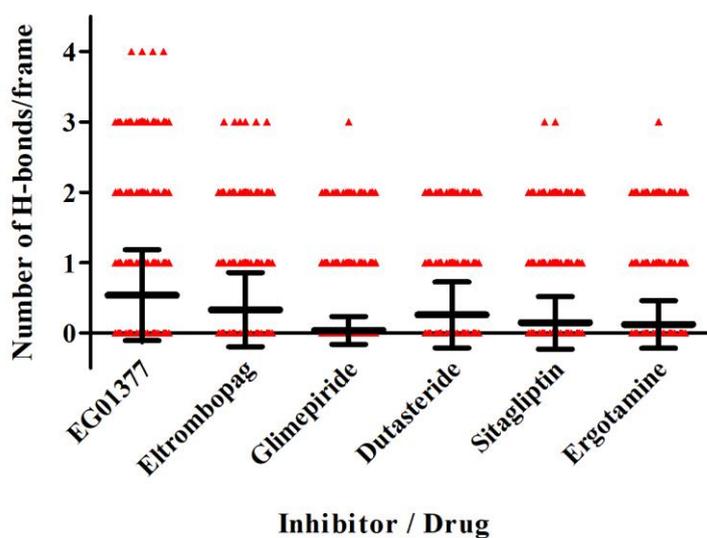
Figure 5. H-bond analysis of each drug/inhibitor made to NRP1 (per frame) in MD simulation. A total of 25000 frames (every 4ps) were included for this calculation.

Table 3: MM/GBSA BFE after Alanine mutations of selected residues

Mutations Drugs	BFE (kcal/mol)			
	Y297A / ΔΔG	W301A / **ΔΔG**	T316A / **ΔΔG**	Y353A / ΔΔG
Eltrombopag	-12.99 / **4.12**	-14.75 / **2.36**	-16.65 / **0.46**	-14.74 / **2.37**
Ergotamine	-12.77 / **2.18**	-12.52 / **2.43**	-14.63 / **0.32**	-13.41 / **1.54**
Sitagliptin	-11.56 / **1.78**	-10.74 / **2.60**	-12.79 / **0.55**	-10.28 / **3.06**
Glimepiride	-11.27 / **1.28**	-11.51 / **1.04**	-12.65 / **-0.10**	-10.16 / **2.39**
Dutasteride	-7.23 / **2.24**	-8.84 / **0.63**	-9.23 / **0.24**	-8.72 / **0.75**
EG01377	-12.16 / **4.03**	-13.09 / **3.1**	-15.44 / **0.75**	-14.03 / **2.16**
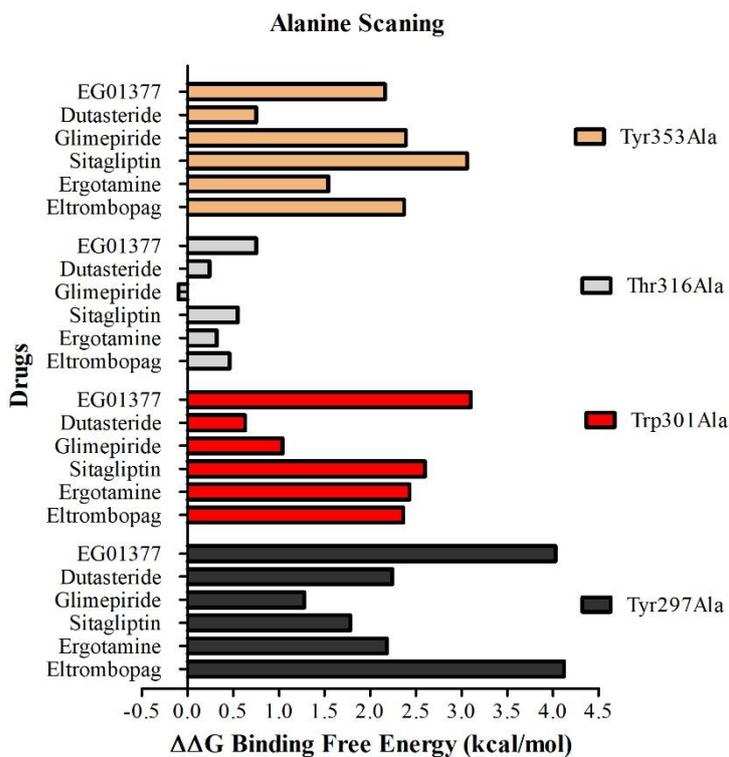
Figure 6. Contribution of critical residues to BFE in drug-NRP1binding.

Histogram of Binding Energy
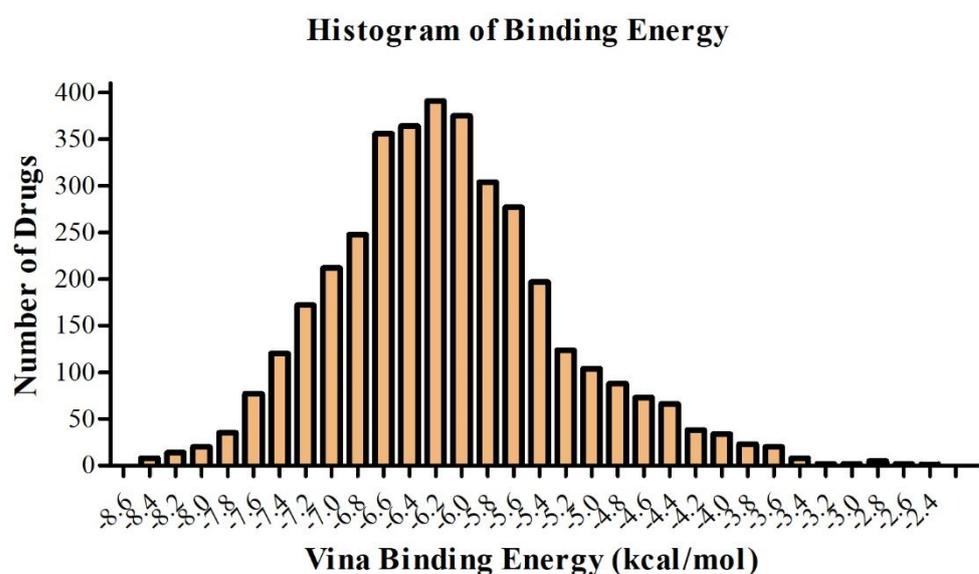
Figure S1. Vina binding energies of all drugs to NRP1

Table S1. Top 100 drugs from docking simulations

Vina Binding Energy (kcal/mol)	ZINC ID	Drug Name	Usage
-8.5	ZINC000011679756	Eltrombopag	Used to treat low blood platelet counts in adults with chronic immune (idiopathic) thrombocytopenia (ITP)
-8.5	ZINC000003830767	Estradiol benzoate	Act as the major female sex hormone
-8.5	ZINC000019632618	Imatinib	A small molecule kinase inhibitor used to treat certain types of cancer.

-8.4	ZINC000064033452	Lumacaftor	Used for the management of Cystic Fibrosis (CF) in patients aged 6 years and older.
-8.4	ZINC000011681563	Netupitant	An antiemitic drug used in combination with palonosetron for the prevention of acute and delayed vomiting and nausea associated with cancer chemotherapy
-8.4	ZINC000036701290	Ponatinib	Ponatinib is a novel Bcr-Abl tyrosine kinase inhibitor that is especially effective against the T315I mutation for the treatment of chronic myeloid leukemia.
-8.3	ZINC000000006157	Epinastine	Used for the prevention of itching associated with allergic conjunctivitis.
-8.3	ZINC000000002070	Sorbinil	Aldose reductase inhibitor
-8.2	ZINC000000537791	Glimepiride	Used for the management of type 2 diabetes mellitus (T2DM) to improve glycemic control.
-8.2	ZINC000003932831	Dutasteride	Novel dual 5α-reductase inhibitor that works by blocking both isoforms of 5α-reductase enzymes in a potent, selective, and irreversible manner.
-8.2	ZINC000001489478	Sitagliptin	A Dipeptidyl peptidase-4 (DPP-4) inhibitor used in conjunction with diet and exercise to improve

			glycemic control in patients with type 2 diabetes mellitus
-8.2	ZINC000000004724	Trileptal	An anti-epileptic medication used in the treatment of partial onset seizures that was first approved for use in the United States in 2000
-8.1	ZINC000001996117	Darifenacin	Used to treat urinary incontinence.
-8.1	ZINC000052955754	Ergotamine	Alpha-1 selective adrenergic agonist and is commonly used in the treatment of migraine disorders.
-8.1	ZINC000002032615	Permethrin	A pyrethroid insecticide commonly used in the treatment of lice infestations and scabies.
-8.1	ZINC000003831448	Silibinin	Has hepatoprotective (antihepatotoxic) properties that protect liver cells against toxins.
-8	ZINC000000119978	Catechin	An antioxidant flavonoid
-8	ZINC000003869855	Dicumarol	Interferes with the metabolism of vitamin K.
-8	ZINC000003978005	Dihydroergotamine	A 9,10alpha-dihydro derivative of ergotamine. It is used as a vasoconstrictor, specifically for the therapy of migraine disorders.

-8	ZINC000003830847	Flubendazole	Flubendazole is an anthelmintic that is used to treat worm infection in humans..
-8	ZINC000000897089	Mefloquine	A phospholipid-interacting antimalarial drug.
-8	ZINC000001540998	Pemetrexed	Use in combination with cisplatin for the treatment of patients with malignant pleural mesothelioma
-8	ZINC000002510358	Phenytoin	One of the most commonly used anticonvulsants.
-8	ZINC000001539579	Targretin	An antineoplastic agent used off-label for lung cancer, breast cancer, and Kaposi's sarcoma.
-7.9	ZINC000012504271	Atovaquone	A hydroxynaphthoquinone, or an analog of ubiquinone, that has antimicrobial and antipneumocystis activity.
-7.9	ZINC000003830772	Estradiol cypionate	Major female sex hormone.
-7.9	ZINC000003824921	Fexofenadine	Antihistamine used in the treatment of various allergic symptoms
-7.9	ZINC000002036732	Florantyrone	Florantyrone is used in the treatment of biliary dyskinesia
-7.9	ZINC000000002272	Ketoprofen	A nonsteroidal anti-inflammatory agent (NSAIA) with analgesic and antipyretic properties

-7.9	ZINC000003831159	Latamoxef	A broad- spectrum beta-lactam antibiotic
-7.9	ZINC000000121541	Mebendazole	Acts by interfering with carbohydrate metabolism and inhibiting polymerization of microtubules.
-7.9	ZINC000003831169	Nafcillin	A semi-synthetic antibiotic related to penicillin
-7.9	ZINC000003816514	Rolapitant	A potent, highly selective, long-acting Neurokinin-1 (NK-1) receptor antagonist
-7.9	ZINC000000004785	Tegretol	Used to control seizures and to treat pain resulting from trigeminal neuralgia
-7.8	ZINC000000896717	Zafirlukast	An oral leukotriene receptor antagonist (LTRA) for the maintenance treatment of asthma
-7.8	ZINC000000009073	Apomorphine	A non-ergoline dopamine D2 agonist indicated to treat hypomobility associated with Parkinson's.
-7.8	ZINC000000968264	Cyproheptadine	A serotonin antagonist and a histamine H1 blocker used as antipruritic
-7.8	ZINC000003830628	Danazol	A synthetic steroid with antigonadotropic and anti-estrogenic activities

-7.8	ZINC000003830765	Estradiol	Estradiol is a naturally occurring hormone circulating endogenously in females.
-7.8	ZINC000003939013	Fosaprepitant	An intravenously administered antiemetic drug.
-7.8	ZINC000005162311	Ilevro	A non-steroidal anti-inflammatory prodrug (NSAID)
-7.8	ZINC000000002279	Ketorolac	A non-steroidal anti-inflammatory drug (NSAID)
-7.8	ZINC000003831231	Novobiocin	An antibiotic compound derived from Streptomyces niveus.
-7.8	ZINC000000897253	Olopatadine	Selective histamine H1 antagonist and mast cell stabilizer
-7.8	ZINC000004175630	Pimozide	An antipsychotic agent, alternative to haloperidol for the suppression of vocal and motor tics in patients with Tourette syndrome.
-7.8	ZINC000000538658	Tolvaptan	Used to treat low blood sodium levels (hyponatremia) associated with various conditions
-7.8	ZINC000006745272	Regorafenib	Regorafenib is an orally-administered inhibitor of multiple kinases.
-7.8	ZINC000000020253	Thalitone	A thiazide-like diuretic used for the treatment of hypertension

-7.7	ZINC000003830716	Diphenoxylate	A meperidine congener used as an antidiarrheal
-7.7	ZINC000027428713	Aprepitant	An antiemetic, P/neurokinin 1 (NK1) receptor antagonist
-7.7	ZINC000000537795	Glipizide	An oral hypoglycemic agent, used to control blood sugar levels in patients with type 2 diabetes mellitus.
-7.7	ZINC000019796080	Droperidol	Used in conjunction with an opioid analgesic such as fentanyl to maintain the patient in a calm state of neuroleptanalgesia
-7.7	ZINC000001550477	Lapatinib	An anti-cancer drug
-7.7	ZINC000000000509	Mirtazapine	A tetracyclic piperazino-azepine antidepressant agent
-7.7	ZINC000004213946	Nebivolol	A racemic mixture of 2 enantiomers where one is a beta adrenergic antagonist and the other acts as a cardiac stimulant without beta adrenergic activity.
-7.7	ZINC000001481956	Paliperidone	The primary active metabolite of risperidone
-7.7	ZINC000003819392	Riociguat	A soluble guanylate cyclase (sGC) agonist
-7.7	ZINC000001493878	Sorafenib	Used for the treatment of advanced renal cell carcinoma (primary kidney cancer).

-7.7	ZINC000004475353	Sulindac	A nonsteroidal anti-inflammatory drug (NSAID) of the arylalkanoic acid class
-7.7	ZINC000003831615	Zeranol	A non-steroidal estrogen agonist.
-7.7	ZINC000000538550	Ziprasidone	Atypical antipsychotics, used to treat schizophrenia and bipolar disorder
-7.6	ZINC000002568036	Dantrolene	A hydantoin derivative but does not exhibit antiepileptic activity
-7.6	ZINC000000403011	Labetalol	Used to treat hypertension
-7.6	ZINC000053151228	Methysergide	An ergot derivative that antagonizes the effects of serotonin in blood vessels and gastrointestinal smooth muscle
-7.6	ZINC000001530977	Naftifine	A synthetic, broad spectrum, antifungal agent
-7.6	ZINC000084589076	Warfarin	An anticoagulant drug normally used to prevent blood clot formation as well as migration.
-7.6	ZINC000000523926	Gliclazide	Used for the treatment of non-insulin-dependent diabetes mellitus (NIDDM).
-7.6	ZINC000003831490	Sulfasalazine	Used in the management of inflammatory bowel diseases.
-7.6	ZINC000001530596	Cephalexin	Used to treat a number of susceptible bacterial infections through inhibition of cell wall synthesis

-7.6	ZINC000001552174	Cilostazol	Quinolinone derivative and antiplatelet agent with vasodilating properties
-7.6	ZINC000000402909	Fenoprofen	An anti-inflammatory analgesic and antipyretic highly bound to plasma proteins.
-7.6	ZINC000000537877	Ketanserin	Investigated for the treatment of Septic Shock, Severe Sepsis, and Diabetic Foot Ulcer.
-7.6	ZINC000003830435	Ceforanide	Second-generation cephalosporin antibiotic
-7.6	ZINC000058581064	Dolutegravir	HIV-1 intergrase inhibitor
-7.6	ZINC000013520815	Estradiol Transdermal Patch	Naturally occurring hormone circulating endogenously in females. Used in several hormone therapy products for managing conditions associated with reduced estrogen
-7.6	ZINC000000000903	Alprazolam	Used for the treatment of anxiety and panic disorders.
-7.6	ZINC000000538505	Trifluperidol	Experimental
-7.6	ZINC000001997125	Pomalidomide	An immunomodulatory antineoplastic agent
-7.6	ZINC000053683151	Bromocriptine	A semisynthetic ergot alkaloid derivative with potent dopaminergic activity.
-7.6	ZINC000003802417	Alvimopan	Peripherally acting μ opioid antagonist.

-7.6	ZINC000000537804	Glisoxepide	sulphonamide-derived oral antidiabetic drug
-7.6	ZINC000009212426	Leucovorin	A necessary co-factor in the body.
-7.6	ZINC000001481983	Benzoctamine	Used as a sedative which does not depress the respiratory system, but rather stimulates it.
-7.6	ZINC000001612996	Irinotecan	Anticancer
-7.6	ZINC000000968337	Azatadine	Antihistamines to compete with histamine for histamine H1-receptor sites on effector cells.
-7.6	ZINC000019632668	Doxapram	A central respiratory stimulant with a brief duration of action
-7.6	ZINC000003830594	Dicloxacillin	One of the penicillins which is resistant to penicillinase
-7.6	ZINC000003830401	Cefatrizine	Experimental
-7.6	ZINC000068202099	Sonidegib	A Hedgehog signaling pathway inhibitor developed as an anticancer agent.
-7.6	ZINC000000057321	Fenoterol	An adrenergic beta-2 agonist that is used as a bronchodilator and tocolytic.
-7.5	ZINC000000086535	Flufenamic Acid	An anthranilic acid derivative with analgesic, anti-inflammatory, and antipyretic properties.
-7.5	ZINC000018067894	Acetohexamid	A sulfonylurea hypoglycemic agent

-7.5	ZINC000000897225	Hidroflumetiazid	A thiazide diuretic with actions and uses similar to those of hydrochlorothiazide
-7.5	ZINC000043207238	Canagliflozin	A sodium-glucose cotransporter 2 (SGLT2) inhibitor used in the management of type 2 diabetes mellitus
-7.5	ZINC000000897408	Bicalutamide	An oral non-steroidal anti-androgen for prostate cancer.
-7.5	ZINC000000004893	Asenapine	Atypical antipsychotic for treatment of schizophrenia and acute mania associated with bipolar disorder.
-7.5	ZINC000035342789	Tolcapone	Used in the treatment of Parkinson's disease as an adjunct to levodopa/carbidopa medication.
-7.5	ZINC000019796168	Sildenafil	Prevents or minimizes the breakdown of cyclic guanosine monophosphate (cGMP) by inhibiting cGMP specific phosphodiesterase type 5 (PDE5) pulmonary hypertension
-7.5	ZINC000003830836	Doxepin	A psychotropic agent with antidepressant and anxiolytic properties
-7.5	ZINC000000001547	Hydroxystilbamidine isethionate	Used in the therapy of some patients with nonprogressive blastomycosis of the skin, and

			pulmonary or systemic blastomycosis in children